



*Journal Homepage: - [www.journalijar.com](http://www.journalijar.com)*

## INTERNATIONAL JOURNAL OF ADVANCED RESEARCH (IJAR)

Article DOI: 10.21474/IJAR01/xxx  
DOI URL: <http://dx.doi.org/10.21474/IJAR01/xxx>

ISSN NO. 2320-5407



**RESEARCH ARTICLE**

**EXPERIMENTAL VALIDATION OF AN ELECTROMAGNETIC JET AT THE OUTPUT OF A  
RECTANGULAR WAVEGUIDE**

**Manuscript Info**

**Manuscript History**

Received: xxxxxxxxxxxxxxxx  
Final Accepted: xxxxxxxxxxxxxx  
Published: xxxxxxxxxxxxxxxx

**Key words:-**

Rectangular WR90 Waveguide,  
Electromagnetic Waves, and Near-Field  
Calibration, photonic jet, electromagnetic jet

**Abstract**

This study explores the generation of electromagnetic jets using a PTFE-loaded rectangular waveguide with an optimally designed tip. Due to the complexity of the structure, an optimization study was conducted to enhance computational efficiency while ensuring accuracy. Two prototypes were fabricated and experimentally tested, with key measurement challenges successfully addressed. The results demonstrate that a PTFE-loaded waveguide can effectively generate an electromagnetic jet, paving the way for potential applications in high-resolution imaging, beam shaping, and advanced electromagnetic wave control.

*Copy Right, IJAR, 2023.. All rights reserved.*

**Introduction:**

Among non-destructive and contactless inspection techniques, near-field measurement in the microwave domain enables the detection and characterization of small defects in materials and devices. Although the inspected areas are significantly smaller than those in far-field methods, the dimensions of the defects sought can be smaller than the wavelength, or in some cases, may exceed the diffraction limit. The principle of these techniques relies on the collection of electromagnetic waves in close proximity to the devices under test using circular [1] or rectangular [2] probes. They thus offer good spatial resolution and are particularly useful for applications such as surface state measurement or the detection of surface and internal defects in materials, provided the materials allow electromagnetic wave penetration. However, since the sample under measurement is placed very close to the probe, this approach presents several challenges, including risks of damage due to contact with the surface and, more importantly, diffraction and interference effects, which are of particular interest in this article.

An innovative solution, known as the photonic jet, was introduced by Chen et al. in 2004 [3]. This technique leverages the interaction between light and a dielectric sphere to achieve near-field focusing, resulting in a full-width at half-maximum (FWHM) smaller than half a wavelength, thus overcoming the conventional diffraction limit [4]. This approach can then be used to perform measurements in an intermediate zone close to the near-field region. Thus, this technology has been implemented in the microwave domain using a parallel plate waveguide [5-6], a horn antenna [7], and a rectangular waveguide [8]. This latter structure is based on an open rectangular waveguide extended by a polytetrafluoroethylene (PTFE) extension, enabling the generation of what has been termed an electromagnetic jet by generalizing the concept of the photonic jet [8]. This configuration concentrates the near-field distribution near the extension, over a spatial region potentially smaller than the diffraction limit.

In this article, we study the numerical and experimental validation procedures for the distribution of electromagnetic fields in a region slightly beyond the near-field zone and demonstrate the possibility of generating an

33 electromagnetic jet in the microwave domain at 15 GHz using a rectangular waveguide equipped with a PTFE  
 34 extension.

35

## 36 RESULTS AND DISCUSSION

### 37 Numerical Results

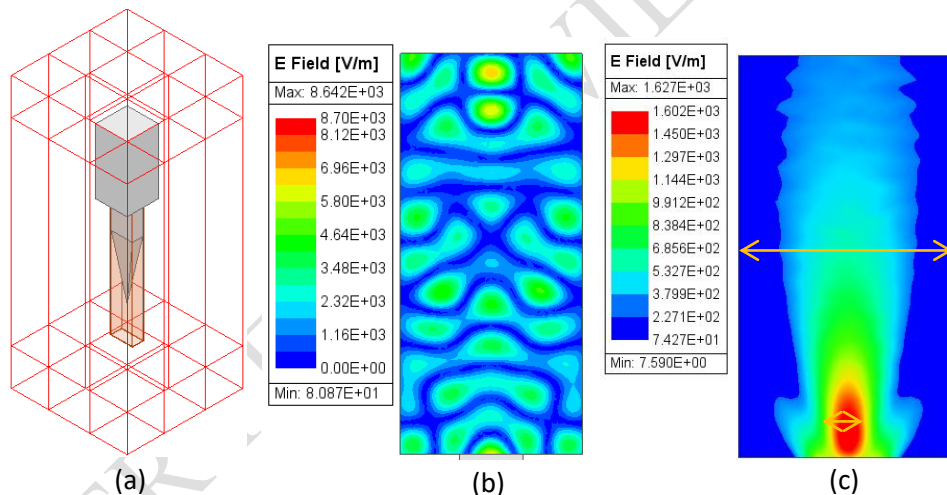
38 The structure consists of a WR90 waveguide equipped with a PTFE extension (Fig. 1a). The waveguide is excited at  
 39 15 GHz by the TE<sub>10</sub> mode. The PTFE extension penetrates inside the waveguide and then tapers into a tip to create  
 40 effective impedance matching between the empty rectangular waveguide and the dielectric-filled waveguide.

41 A full-wave simulation of the structure and its radiation outside is performed using an electromagnetic simulator  
 42 based on the finite element method. To reduce the computational volume and avoid potential wave reflections at the  
 43 computational boundaries, absorbing layers known as Perfectly Matched Layers (PML) are applied at the limits of  
 44 the computational space. This technique is based on the impedance matching condition between two media with the  
 45 same refractive index, one of which is absorbing. This modeling method saves computational time by reducing the  
 46 volume to be discretized. Figure 1 illustrates the simulation results of the complete structure.

47

48 The rectangular structure is presented (Fig. 1a) with its free-space computational domain, represented by the outer  
 49 box in red dashed lines. Figure 1b shows the results obtained with simple free-space radiation conditions; a standing  
 50 wave regime is observed, which does not converge to the expected response. In contrast, Figure 1c, obtained with  
 51 PML for the same mesh, offers much better results. The analysis of Figure 1c allows for a correct visualization of  
 52 the field distribution outside the structure. A strong field concentration zone is observed at the output of the PTFE  
 53 tip. This focal zone is intense and narrow, smaller than the wavelength. The -3dB limit is indeed delimited by the  
 54 yellow contour (the total width of Figure 1c represents  $4.75\lambda$ ).

55



56

57 **Fig.1:** Modelling a rectangular waveguide with a rectangular-section PTFE extension and its impedance  
 58 adaptation. (a) 3D structure bounded by Perfectly Matched Layers, (b) free-space distribution with simple  
 59 radiative condition and (c) with PML

### 60 Experimental Results

61 To validate the accuracy of the simulation results, the presented device was fabricated, and an experimental study  
 62 was conducted.

63

64 The measurement bench used (Fig. 2) to characterize the electric field distribution at the output of the PTFE  
 65 extension consists of the rectangular waveguide equipped with its PTFE extension on the emitting side and a field  
 66 probe made from an open empty rectangular waveguide on the receiving side. Both the PTFE-loaded waveguide and  
 67 the probe are connected to a Vector Network Analyzer (VNA). On the emitting side, the loaded waveguide is fixed  
 68 on a stationary support, and on the receiving side, the probe is positioned on a two-axis robotic arm, allowing for the  
 69 probing of the desired planes at the output of the PTFE extension.

70

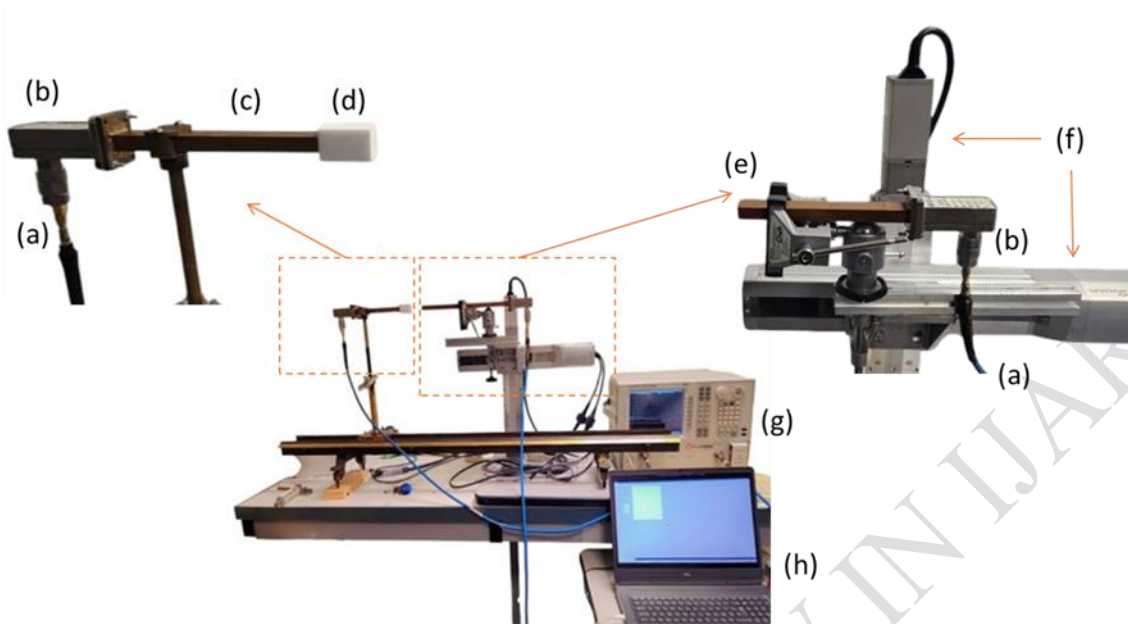


**Fig. 2:** Experimental setup for mapping the electromagnetic field generated at the end of the PTFE extension of the rectangular waveguide. (a) coaxial cable (b) WR/Coaxial transition (c) rectangular waveguide (d) PTFE tip (e) open rectangular guide probe (f) two-axis robotic arm (g) VNA (h) Control PC.

The VNA is first calibrated at the end of the coaxial cables to minimize losses and errors in the measurement system. The prototype, labeled as Prototype No. 1 and depicted in Figure 3a, was subsequently tested on the measurement bench. The results of this test, shown in Figure 3b, illustrate the measurements obtained during the scanning of the space at the output of the PTFE tip by the probe. A standing wave is clearly visible, superimposed on the field generated by the device, which degrades the experimental acquisition of the electric field distribution at the output.

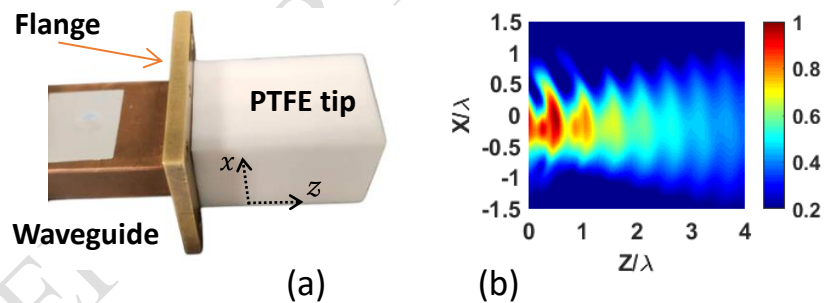


**Fig. 3:** (a) 3D view of Prototype No. 1, illustrating the waveguide equipped with a flange terminated by a PTFE tip. (b) Measurements of the normalized electric field intensity distribution ( $|E|^2$ ) in free space at the output of the rectangular waveguide with a PTFE extension, for a frequency of 15 GHz.

We then sought the elements that could be the origin of this phenomenon. As seen in Figure 3a, the connecting flange of the rectangular waveguide is bulky and significantly protrudes from the PTFE tip. To improve the result, the flange was cut to obtain prototype N°2, as depicted in Figure 4a. The mapping of this second prototype was then performed, and the results are presented in Figure 4b. These results show that the standing wave has been significantly reduced compared to prototype N°1. A spatial distribution closer to the simulation results is now observed. However, parasitic phenomena remain, notably a split focal zone, indicative of destructive interference at the center of the intended focus.

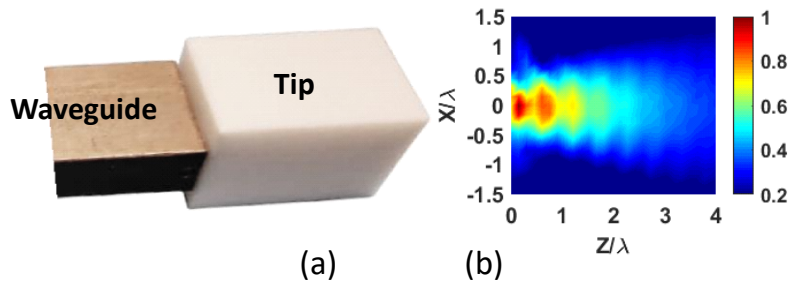


**Fig. 4:** (a) 3D view of Prototype No. 2 illustrating the waveguide without a flange, terminated by a PTFE tip. (b) Measurements of the normalized electric field intensity distribution ( $|E|^2$ ) in free space at the output of the rectangular waveguide with a PTFE extension, for a frequency of 15 GHz.

93  
94  
95  
96

97 These perturbations originate from the measurement bench environment. To eliminate them, we implemented a  
98 calibration method for external elements, inspired by techniques used in far-field measurements. We opted for a TRL  
99 calibration [9] based on the *Thru* (a direct connection between the two ports), *Reflect* (a short-circuit measurement  
100 using a metal plate), and *Line* (a transmission line of a determined length) standards. This method requires several  
101 steps, illustrated in Figure 5.

102 First, we measure the reflection coefficients (Reflect), which involves placing a short circuit (in this case, a large  
103 metal plate) between port 1 and port 2 (Fig. 5a). The metal plate is placed at a distance  $a$ , corresponding to the focus  
104 of the electromagnetic jet. Subsequently, port 2 is calibrated using the same short circuit (Fig. 5b). The next  
105 step involves establishing a direct connection between the two ports, as illustrated in Figure 5c. Finally, in the Line  
106 step (Fig. 5d), ports 1 and 2 are positioned at a distance of  $2a$  plus a quarter of the wavelength ( $\lambda/4$ ), which is  
107 determined by the operating frequency.

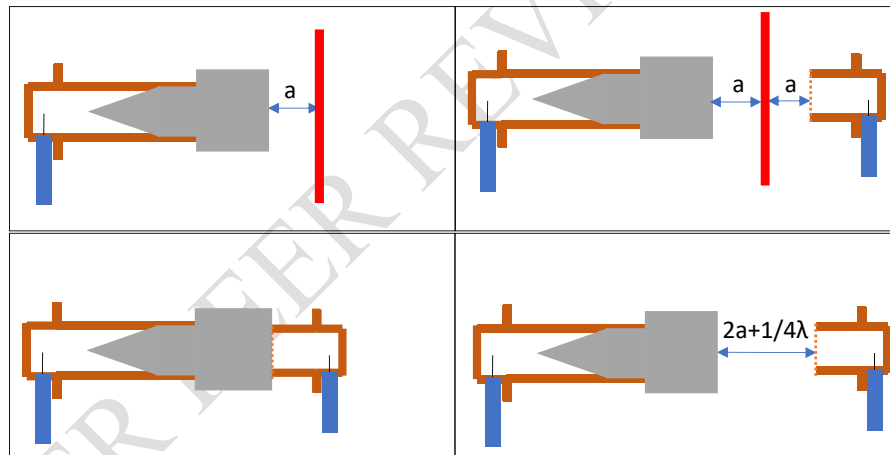


**Fig.5:** Calibration Procedure. (a) Reflect for port 1 (b) Reflect for port N°2 (c) Thru (d) Line.

108  
109

110 The spatial distribution of the electric field of prototype N°2 (Fig. 4a) was measured again following the established  
111 protocol. The results, depicted in Figure 6b, demonstrate a significant improvement, with a further reduction of the  
112 standing waves superimposed on the measurement. Notably, the focal zone is no longer divided into two parts, as  
113 previously observed in Figure 5b. The measurements now exhibit good agreement with the simulation results (Fig.  
114 6a), particularly in terms of the  $-3\text{dB}$  width along the  $x$ -direction.

115  
116

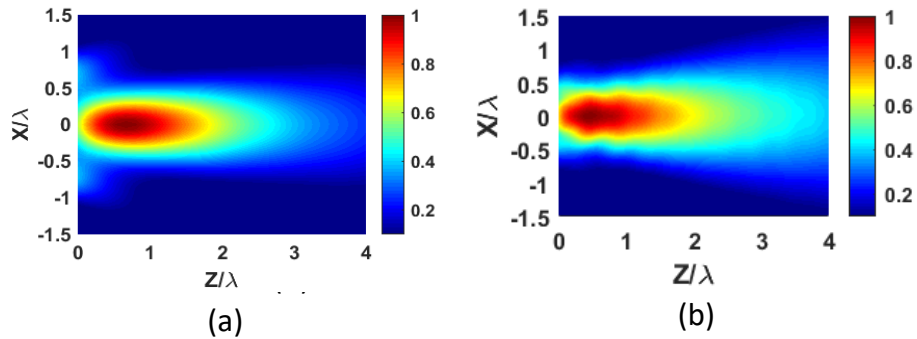


**Fig.6:** Mapping of the normalized transverse electric field intensity in the plane defined by the propagation direction ( $z$ ) and the vertical polarization of the excitation ( $x$ ): (a) simulated mapping and (b) Measured mapping.

From the intensities obtained in Figure 6b, we deduced the amplitude of the electric field (Fig. 7). This clearly reveals wavefronts that, over a width smaller than the wavelength (along the  $x$ -axis), can be considered quasi-planar over a distance of 2 or 3 wavelengths along the  $z$ -axis. This observation, combined with the strong intensity at the focus, allows the phenomenon to be qualified as an electromagnetic jet according to the criteria given in [4].

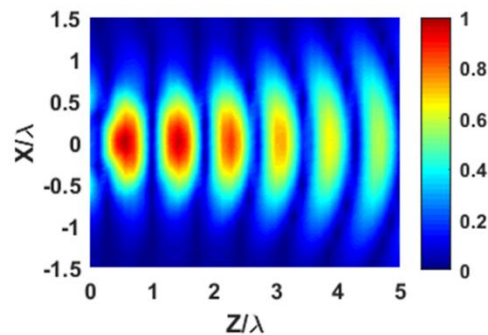


**Fig.7:** Measured amplitude of the electric field in the plane defined by the propagation direction ( $z$ ) and the vertical polarization of the excitation ( $x$ ) at 15GHz.

Based on the intensities shown in Figure 6b, the amplitude of the electric field was derived (Fig. 7). The results distinctly reveal wavefronts that, over a width smaller than the wavelength (along the  $x$ -axis), can be regarded as quasi-planar across a distance of 2 to 3 wavelengths along the  $z$ -axis. This behavior, coupled with the high intensity observed at the focal point, meets the criteria outlined in [4] for characterizing the phenomenon as an electromagnetic jet.

### Conclusion:

An open WR90 rectangular waveguide, operating in the frequency band from 8.2 GHz to 12.4 GHz, was studied to generate an electromagnetic jet in the near field at 15 GHz.

Given the complexity of the structure under study, it must be fully modeled, starting from the empty waveguide, passing through the matching tip, the loaded waveguide, and the PTFE tip, to observe what happens in the space near the near-field zone. Due to the size of the model to be simulated, a study was conducted to balance computational efficiency and accuracy. To ensure good convergence while minimizing computational volume, Perfectly Matched Layer (PML) boundary conditions were employed, yielding satisfactory results.

Two prototypes were fabricated and experimentally tested. The major issue encountered was the perturbation of the measurement by standing waves. To mitigate this issue, prototype N°2 was designed, removing connecting flange of the rectangular waveguide. Additionally, the implementation of TRL calibration, alongside VNA calibration, significantly improved measurement accuracy, leading to strong agreement between simulation and experimental field mapping results.

Through both simulation and experimental validation, we have demonstrated that an electromagnetic jet can be effectively generated using a PTFE-loaded rectangular waveguide with an appropriately designed tip.

152

153 **References:**

- 154 [1] Ramzi, M. R., Abou-Khousa, M., & Prayudi, I. (2017). Near-field microwave imaging using open-ended  
155 circular waveguide probes. *IEEE sensors journal*, 17(8), 2359-2366.
- 156 [2] Qaddoumi, N. N., Abou-Khousa, M. et Saleh, W. M. (2006). Near-field microwave imaging utilizing tapered  
157 rectangular waveguides. *IEEE transactions on instrumentation and measurement*, 55(5), 1752-1756.
- 158 [3] Z. Chen, A. Taflove, et V. Backman, « Photonic nanojet enhancement of backscattering of light by nanoparticles:  
159 a potential novel visible-light ultramicroscopy technique », *Opt. Express*, vol. 12, no 7, p. 1214, 2004, doi:  
160 10.1364/OPEX.12.001214.
- 161 [4] Lecler, S., Takakura, Y., & Meyrueis, P. (2005). Properties of a three-dimensional photonic jet. *Optics letters*,  
162 30(19), 2641-2643.
- 163 [5] B. Ounnas, B. Sauviac, Y. Takakura, S. Lecler, B. Bayard, et S. Robert, « Single and Dual Photonic Jets and  
164 Corresponding Backscattering Enhancement with Tipped Waveguides: Direct Observation at Microwave  
165 Frequencies », *IEEE Trans. Antennas Propagat.*, vol. 63, no 12, p. 5612-5618, dec. 2015, doi:  
166 10.1109/TAP.2015.2491328.
- 167 [6] H. Hyani, B. Sauviac, G. Granet, B. Bayard, S. Robert, and K. Edee, “Electromagnetic jet produced with loaded  
168 waveguide ended by an optimized multi-rectangular sections tip,” *Journal of Electromagnetic Waves and  
169 Applications*, pp. 1–10, Sep. 2023, doi: 10.1080/09205071.2023.2262984.
- 170 [7] M. Granger, A. Ghaddar, B. Bayard, and B. Sauviac, “Toward Free Space Local Characterization Method in  
171 Microwave,” presented at the IEEE MTT-S International Microwave Symposium, Washington, DC, USA, Jun.  
172 2024. doi: 10.1109/IMS40175.2024.10600270.
- 173 [8] B. Sauviac, A. Ghaddar, A. Deubaibe, H. Hyani, and B. Bayard, “Toward microwave electromagnetic jets for  
174 detection, imaging, and local characterization applications,” in *Nanophotonics X*, Strasbourg, France, Apr. 2024.
- 175 [9] G. F. Engen and C. A. Hoer, “Thru-reflect-line: An improved technique for calibrating the dual, six-port  
176 automatic network analyzer,” *IEEE transactions on microwave theory and techniques*, vol. 27, no. 12, pp. 987–  
177 993, 1979.